An experimental analysis of fracture mechanisms by acoustic emission of woven composite bolted assembly

---

Analyse expérimentale des mécanismes de rupture par émission acoustique des assemblages boulonnés en composite tissé

Youcef Faci[*1] & Mostefa Baccouche[2]

[1]*Centre Nationale de recherche scientifique et technique en soudage et Contrôle,
BP 64, Route Dely Brahim, Cheraga 16000, Alger, Algérie.*

[2]*Laboratoire de Métallurgie physique et Propriété des Matériaux, Université Badji Mokhta,r
BP 12, Annaba, 23000. Algérie.*

ملخص

يقترح هذا العمل دراسة تطور الوسائط التالفة وآليات انكسار جمعية انسحب المركبة من ألياف الكربون المنسوجة/الايبوكسي. تمت دراسة ثلاثة تكوينات تتمثل في [0°، 45°، 0، 45°]، [0°]،[°45 ،°0 ،°45 ،°0] و [0° ، 45° ، 0 ، °45 ، °0]ₛ. ومن أجل تحليل سلوك الميكانيكي للجمعية ، تمت اختبارات الشدة مفردة النغمة. ويتبع تطور التلف عن طريق الانبعاثات الصوتية (E.A) وارتباط الصورة الرقمية (D.I.C) في وقت واحد. التوقيعات الصوتية لأنواع التلف ا لأربعة تمت معاينتها وهي كالتالي , القوالب المتشققة، اللاتماسك (الألياف- القالب) ، الألياف مصفوفة التبطين، وأخيرا تفكيك الألياف. ثم أكدته الملاحظات المجهرية باستعمال المجهرالإلكتروني المختص في المسح (S.E.M)

الكلمات المفتاحية :ألياف الكربون المنسوجة - الانبعاثات الصوتية - جمعية بولت - ارتباط الصورة الرقمية - التلف.

Abstract

This work is focused on the study of the evolution of damage mode and failure mechanisms of woven composite bolted assembly carbon fiber/epoxy. In the present paper three configurations are studied [0°,45°,0°,45°], [0°,45°,0°,45°]ₛ and [0°,45°,0°,45,0°]ₛ. In order to analyze a global mechanical behavior of the assembly, monotonous tensile tests are performed. The damage evolution is followed simultaneously by acoustic emission (A.E) and digital image correlation (D.I.C). Acoustic signatures of four modes of damage are identified, matrix cracking, fiber-matrix debonding, delaminating and fiber breakage, then confirmed by microscopic observations in scanning electron microscopy (SEM).

Keywords: woven composite- acoustic emission- bolted assembly- digital image correlation- damage.

Résumé

Ce travail étudie l'évolution des modes d'endommagement et les mécanismes de rupture d'un assemblage boulonnée en composite tissée fibre de carbone/époxy. Trois types de   configurations sont étudiées : [0°,45°,0°,45°], [0°,45°,0°,45°]s et [0°,45°,0°,45°,0°]s. Afin d'analyser le comportement mécanique globale de l'assemblage, des essais de traction monotone sont effectuées. L'évolution de l'endommagement est suivie simultanément par émission acoustique (A.E) et par la corrélation d'image numérique (D.I.C). Les signatures acoustiques des quatre modes d'endommagement sont identifiées à savoir la fissuration matricielle, la décohésion fibre-matrice, le délaminage et enfin la rupture des fibres puis confirmées par des observations microscopiques au microscope électronique à balayage (MEB).

Mots-clés : composite woven, émission acoustique, assemblage boulonné, corrélation d'image   numérique, endommagement.

---

* *Corresponding author: y.faci@csc.dz*

1. INTRODUCTION

Composite materials find more applications in the realization of structural parts of various dimensions in many industries such as aerospace, car manufacturing, nuclear, biomedical engineering. Due to their high specific properties, woven composites carbons (fiber/epoxy) are increasingly used in aerospace applications. These applications generally require the use of assemblies to load transfer between the laminates composite and other parts that are either metallic or composites. However, the design of assemblies remains a hard point for structural applications. Indeed, the use of bonded assemblies is often prohibited by industrial requirements of reproducibility and maintenance. Mechanically-fastened bolted-joints under tensile loads frequently are damaged in five common failure modes (fig.1), namely cleavage, bearing, shear, tension, and pull-through. Cleavage failures are associated with both an inadequate end distance and too few transverse plies, Bearing failure occurs predominantly when the bolt diameter is a small fraction of the plate width, this mode of failure leads to an elongation of the hole. Shear-out failure can be regarded as a special case of bearing failure, this mode of failure can occur at very large end distances for highly orthotropic laminates.Net-tension failure occurs when the bolt diameter is a large fraction of the strip width; this fraction depends on the type of material and lay-up used... Pull-through failure occurs mainly with countersunk fasteners or when the thickness to diameter ratio is sufficiently high to precipitate failure [1-22]. Many studies have attempted to develop methods for understanding these mechanisms using digital image correlation and acoustic emission. The spatial resolution of the aforementioned procedures is relatively poor. Digital image correlation (DIC) has improved the spatial resolution of optical full-field strain measurements. Parsons et al. [7-9] obtained strain fields on two sides of rectangular tensile specimens with this technique using one camera and a right-angle prism. De Almeida et al. [9] recently used one camera and a mirror to measure strain fields on both the front and the lateral side of a specimen simultaneously However, all the methods mentioned above are based on the assumption that the strains measured on the surface of the specimen are representative of the strains throughout the thickness of the specimen, i.e. the reduction of width measured on the front surface is representative for the width reduction throughout the thickness [6]. The most significant parameter used in acoustic emission signals is the amplitude. The works of Chen Karandikar and al. [23] , Kim and Lee [24], Kargers–Kocsis and al [25], Kotsikos and al.[26] ,Ceysson and al [27] , Benzeggagh and al.[28] , Mouhmid and al [29], on different families of composites and on the tensile stress, on bending static or on fatigue show the interest of using this acoustic parameter. However, it is clear that the absolute amplitude values of involved areas vary from one test and material type to another. Uenoya [30] studied the signals in functions of their amplitude and rise time, four zones were identified; matrix cracking, fiber-matrix debonding, delamination and finally fiber breakage. Another parameter was analyzed by Hill [31] on composite glass/epoxy and carbon epoxy; in fact it is a matter of the influence of the energy and amplitude signals in a purpose of predicting failure in composite materials. Huguet and Godin [32-33] have conducted a conventional parametric analysis such as the amplitude, rise time, duration and energy of acoustic emission signals during a monotonous tensile test on unidirectional composites at matrix reinforced by glass fibers.

This work concerns the study of damage and rupture under monotonic loading in tensile test of a carbon fiber reinforced epoxy laminated composite bolted joints with clearance between bolt diameter and hole diameter. The influence of stacking sequences and various geometric parameters of laminates will be taken into account for the study of global mechanical behavior of assembly. For this propose three different stacking sequences and geometries were studied and correspond to specimen A, B and C. Two experimental techniques have been used such as acoustic emission (A.E) and digital image correlation (D.I.C). These two techniques are coupled with the evolution of the load applied with the displacement for improvement identification of different phases as well as the chronology of damage. Complementary microscopic observations (S.E.M) were carried out on post mortem of specimen C. This enables the confirmation of results obtained by two techniques mentioned earlier.
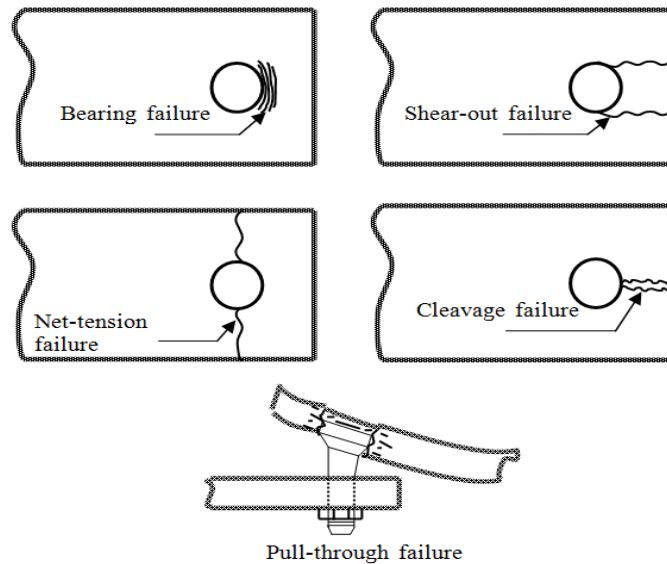
Figure.1: Failure modes of a bolt loaded hole.

2. EXPERIMENTAL PROCEDURES

2.1. Material

The material studied is a laminated composite carbon fiber/epoxy G803/914, based on epoxy resin reinforced by a long carbon fibers fabric. Resin 914 is commonly used in aeronautic field for structures resisting at high temperatures. Mechanical characteristics are specified in table 1.

The reinforcement G/803 is a balanced fabric of carbon fibers of high resistance strength (HR). There manufacture of the fiber by spinning and stretching process may influence the molecules of the material in preferred directions and thus create a mechanical anisotropy fiber. The behavior of the fiber in the longitudinal direction is elastic and brittle, its strain at break of up to 1.4%. Each layer of this dry unidirectional fabric has a thickness of 0.13 mm. Table 2 shows the main features mechanical fibers, where x,y and z indices refer respectively the longitudinal, transversal and perpendicular direction respectively. The mechanical properties of the composite G803/914 are gathered in the table 3.

The mechanical properties of the epoxy matrix, fibers T300 and the composite G803/914 cited previously are provided by the supplier Hexcel Composites. The properties of preimpregnated G803/914 are summarized in table 4.

To determine the effects of joint geometry and stacking sequence on the failure behavior parametric studies were performed experimentally. Therefore, laminated plates were arranged as three stacking sequences named as Groups A, B and C (Tab. 5).

Table.1: Mechanical properties of epoxy matrix Vicotex 914

Young's modulus E	Poisson's ratio N	shear modulus G	Tensile strength yield σ^t_{max}	Elongation at yield ε^t_{max}	Toughnes G_{Ic}	Density P
3.9 GPa	0.41	1.4 GPa	47.7 MPa	0.015	103 J/m^3	1300 Kg/m^3

Table.2: Mechanical properties of fibers T300

E_x	E_y	G_y	σ^t_{max}	ε^t_{max}	P
230 GPa	21 GPa	8.3 GPa	3500 MPa	0.014	1760 Kg/m^3

Table.3**:** Mechanical properties of the composite G803/914.

$E_x = E_y$	E_z	G_{xy}	$G_{xz} = G_{yz}$	ν_{xy}	$\nu_{xz} = \nu_{yz}$
60.3 GPa	5.0 GPa	5.0 GPa	5.0 GPa	0.03	0.35

Table.4**:** the properties of pre-impregnated G803/914

Number of fibers by lock	T300 3K		300
Section of the basic yarn	T300 3K		0.11 mm^2
Linear Mass of the basic yarn	T300 3K	m_l	198 tex (1tex=1g/1000m)
Structure of the fabric	G803		Satin 5
Surface mass of the fabric	G803		295 g/m^2
Surface mass of pre-peg	G803/914	m_s	491 g/m^2
Thickness of polymerized layer	G803/914	e_p	0.308 mm
Mass fraction of fiber in the pre-peg layer	G803/914	f_m	42%
Mass fraction of fibers in the pre-peg layer (value calculated from f_m)	G803/914	f_y	50.5%

Table.5**:** Stacking sequences with the following geometric parameters D (D hole diameter) and q thickness of substrate).

Specimen	Stacking sequences	Thickness q (mm)	D/q
A	[0°,45°,0°,45°]	1.4	4.4
B	[0°,45°,0°,45°] $_s$	2.5	2.48
C	[0°,45°,0°,45°,0°]$_s$	3.22	1.93

The bolted joint of the specimen C is shown on figure 2. It is constituted from two substrates of carbon fiber/epoxy (Fig.2 (1) and Fig. 2(2)) and assembled by bolt and screw (Fig.2 (3) and Fig. 2(4)) used in aeronautic. The fastener respect the recommendation EN-6115-4 (1/4-28 UNJF83-3A). The configuration standard used in this study corresponds to the scope of mechanical assemblies according to the standards ASTM D 5931/D 5961M-962 and [MILHDBK-17-3F]. The edge distance to diameter ratio (e/D=2.57), width to diameter ratio (w/D=5.65) and the total length L = 238.8 mm are fixed for all specimen. Meanwhile reports namely diameter to thickness ratio (D/q) is variable as well as the stacking sequences (Tab. 5). The tightening torque applied is 2.5 daN, with a fixed set of 0.08 mm for all joints. During this experimental study, five tests were carried out and average bearing strength values were computed for each group. Additionally, every bolted-joint was loaded up to the breaking down of the specimen.
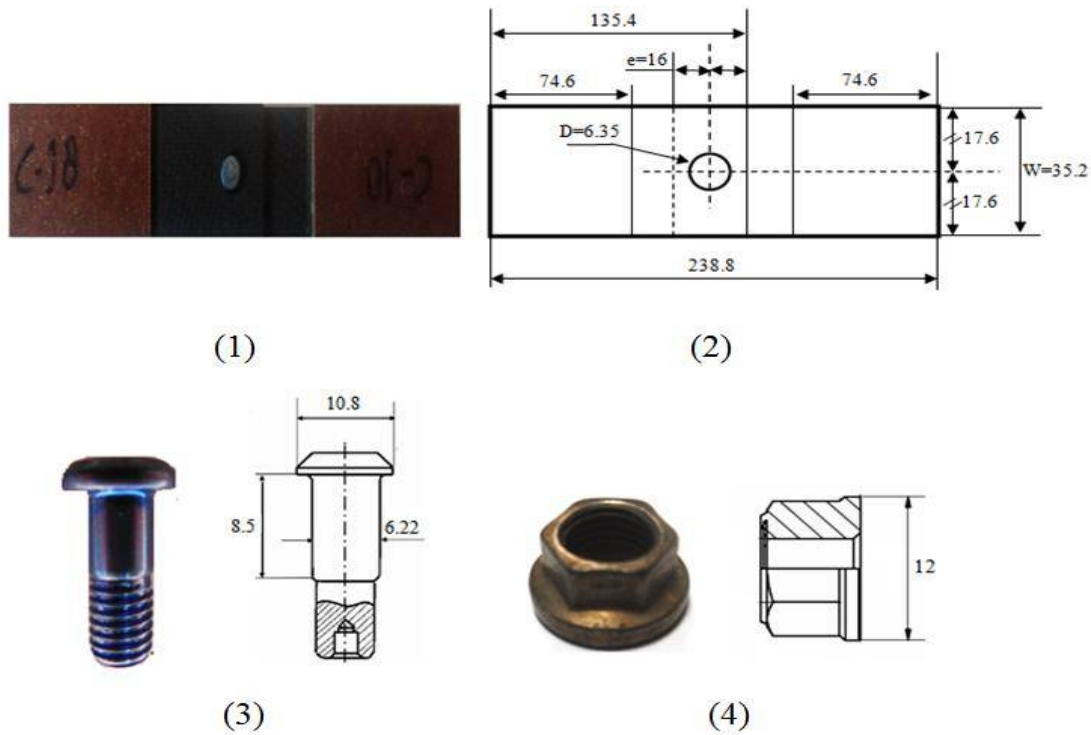
Figure.2: Specimen C, (1) single lap assembly, (2) dimensions of specimen (mm), (3) dimensions of screw in mm, (4) nut and dimensions in mm.

2.2. Experimental technics

To determine the global mechanical characteristics, the monotonic tensile shear was carried out on an electromechanical tensile testing machine, with a displacement rate of the cross-piece of 1 mm/min. The load versus displacement curves for all composite configurations were drawn via a computer connected to the test machine. To check the reproducibility of the tests, five specimens were tested for each group until failure. Two techniques were used simultaneously A.E and C.I.D. Figures. 3 (1) and 3(2) show details of the two techniques as well as the experimental devices. The coupling of A.E. and D.I.C. allows us to identify the various phases of the global behaviour and the chronology of damage in bolted joint assemblies.
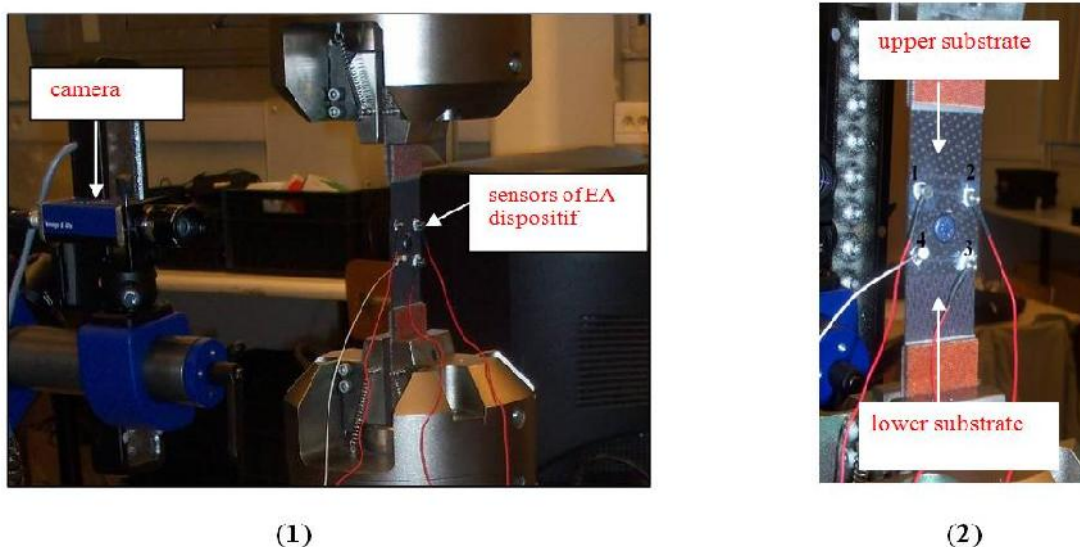

Figure.3: (1) Instron tensile machine with EA and D.I.C dispositifs, (2) Sensors positions.

2.2.1 Digital image correlation

The DIC technique, developed in the 1980s [34–36], consists of displacement and strain determination. Since that, it has been used in various fields. At each load step, an image, corresponding to a given state of deformation, is taken with a CCD camera and digitalized. It is then compared to the undeformed state image (reference image) using a mathematical correlation function. The image processing uses the integral method (comparison of the images with the first image known as reference) with a step of five images per second and window size of 32 x 32 pixels (covering 50%). The pictures resolution used is 28 μm. Displacements and strains could then be calculated at every characteristic point of the studied region.

Among full field measurement techniques, Digital Image Correlation (DIC) is fast emerging because of its versatility and simplicity of use [37]. It consists in evaluating displacement fields corresponding to a series of (white light) pictures taken at distinct stages of loading. If the natural texture of the material is not sufficient for tracking accurately the displacements, a random speckle is usually sprayed onto the surface. Two gray level images I and h (I stands for the reference picture and h that corresponding to the deformed stage) are related through the local passive advection of the texture by a displacement field u:

$$h(x) = I(x + u(x)) \quad (1)$$

The problem consists in identifying the best displacement field by minimizing the correlation residual $\int \varphi^2 dx$ over the whole region of interest, where

$$\varphi(x) = \left| I(x + u(x)) - h(x) \right| \quad (2)$$

The minimization of φ is intrinsically a non-linear and ill-posed problem. For these reasons, a weak form is preferred by adopting a general discretization scheme

$$u(x) = \sum_{n \in N} u_n \psi_n = [\psi(x)]\{u\} \quad (3)$$

Where ψ_n are the vector shape functions and u_n their associated degrees of freedom. In a matrix–vector format,$[\psi]$ is a row vector containing the values of the shape functions ψ_n, and {u} the column vector of the degrees of freedom. After integration over the domain Ω, the global residual is defined as:

$$\phi = \iint_\Omega \left| I(x + [\psi(x)]\{u\}) - h(x) \right|^2 dx \quad (4)$$

At this level of generality, one may choose to decompose the displacement field on a ''mechanically meaningful'' basis. When no simple behavior is expected, one may use a ''simple'' Finite Element kinematic basis. Here, classical bilinear shape functions associated with quadrilateral 4-node elements (or Q4) are chosen. It is referred to as Q4 Digital Image Correlation (or Q4-DIC). The measured displacement fields are next used as inputs for an independent damage law identification procedure, based on the same kinematic description.

2.2.2 Acoustic emission technique (A.E)

The acoustic emission (AE) is a technique that allows studying the phenomena of energy release in the form of transient elastic waves, resulting from internal micro local displacement in a material subjected to stresses (AFNOR NFA 09350 Standard) [32]. The exploitation of the various A.E parameters as showed in figure 4 allows the identification of different phases and propagation of defects. EA software locates the origin of the events, this technique requires specific instrumentation. The device consists of an acquisition system, four sensors piezoelectric and a preamplifier. The threshold value is fixed at 40 dB_{AE}. Acoustic emission signals are registered by four differential sensors piezoelectric type Micro-80, the bandwidth is ranging between 100KHZ to 1 MHz. The sensor diameter is 2 mm, stuck to the specimen with silicone grease. The signals are then amplified with 40 dB, converted through the software and finally scanned to obtain various parameters of acoustic emission.
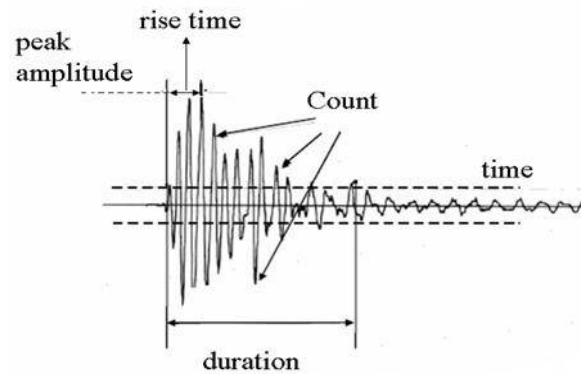
Figure.4: Parameters of acoustic emission.

2.2.3 Location of acoustic events

The location is to determine the coordinates of the area where acoustic event has occurred. Thus, the use of sensors allows the location of acoustic output source (Fig.5 (1)). The most commonly used method is to measure the differences in arrival time (ΔT) of the same signal to a plurality of sensors distributed over the structure. The measurement of (ΔT) is usually triggered by the arrival of the acoustic emission sensor reaches the first wave and closed by its passage of last sensor [38]. When the difference in time of arrival of the same signal is given for four sensors, the locus of points at which the source belongs is defined by:

$$V. \Delta T = const \qquad (1)$$

Where, v is the velocity of wave propagation, assumed to be constant whatever the direction and distance of propagation.

For elastic wave propagation in substrate, with the increase of propagation distance, the amplitude of vibration and the energy reduce gradually. The acoustic signals were acquired at four spatially separate points using acoustic sensors mounted on the substrate in rectangular array as shown in figure 5. The sensors captured signals are mathematically modeled as:

$$\begin{bmatrix} S_1(t) = F(t) + g_1(t) \\ S_2(t) = \partial F(t - M_1) + g_2(t) \\ S_3(t) = \partial F(t - M_2) + g_3(t) \\ S_4(t) = \partial F(t - M_3) + g_4(t) \end{bmatrix} \qquad (2)$$

where S1(t) - S4(t) are sensors outputs, F(t) is the AE source signal, g1(t) - n4(t) are un-

wanted signals, ∂ is attenuation factor caused by the acoustic path differences and D1-D3 are time differences. In this study, the geometrical coordinates of S1 position
Is considered as (0, 0) and others are chosen following S1. The position of AE source is
O(x, y). The sensor-source distances can be obtained by:

$$\begin{bmatrix} O_1 = V \times t_1 \\ O_2 = V \times t_2 \\ O_3 = V \times t_3 \\ O_4 = V \times t_4 \end{bmatrix} \qquad (3)$$

V is the value of propagation velocity, it is the time of propagation of waves from acoustic emission source to sensor Si. The time-delay of propagation of acoustic waves from acoustic source to S1 and S2 can be determined as:

$$\Delta t_1 = t_1 - t_2 = \frac{O_1 - O_2}{V} \qquad (4)$$

in AE source localization propagation velocity and wave arrival times are the most important parameters. The time delay between two collected signals (P1(t), P2(t)) can be determined using cross correlation-function as:

$$R_{P_1 P_2}(\tau) = \sum_{t=1}^{T} p_1(t) p_2(t + \tau) \qquad (5)$$

The parameter (τ) (which maximizes the cross-correlation function $R_{p_1 p_2}(\tau)$ provides an estimation of time delay. In Eq. (3) it is found that a constant wave velocity in substrate must be known in order to locate acoustic emission source.
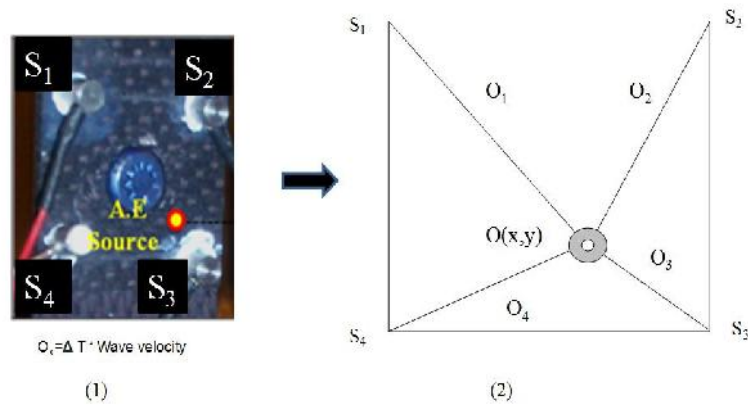
Figure.5. (1) location of acoustic output source, (2) Sensors and acoustic source position for 4 channel position, O(x,y) acoustic source position, and O_1, O_2, O_3, O_4 represent the sensor-to-source distances

3. RESULTS AND ANALYSIS

Figure 6 illustrates the evolution of the load versus displacement of three types of samples with photos of post-mortem tested specimen. The load displacement curve of the test of piece A is characterized by a drop in rigidity of the assembly just after the first peak at 4632 N. The load generally reaches the value ranging between 1 and 5 mm displacements. The observed failure mode of specimen A is the fastener shear out (Fig.7.(1)). This mode of failure is influenced by the form of screw heat and weak thickness of the substrate. The initiated damage according to the specimen A is shown at 83% of final bearing failure. The curve shape of the load versus displacement according to the specimens B is characterized by an increase in the rigidity of the joint just after the first peak. FPS followed by a further stress build-up. This response is characteristic for a progressive failure. According to the definition of failure modes (Fig. 1), the observed failure of laminate B starts as a bearing failure. During the stress build-up between the FPS and the second peak stress (SPS), the damage propagates in a progressive manner. At the SPS, the damage has reached beyond the head of screw and the stress starts declining continuously. The failure mode of the specimen B consists from a combination of bearing and net-tension with a maximum force around 9800 N and a corresponding local displacement of 2.63 mm. (Fig.7. (2)). More energy appears to be required to propagate the shear cracks through the 45°, presente in this laminate B. Experimental test has shown initial damage occured at 61% of final bearing failure. According to the specimen C, the maximum force is around 11800 N with a corresponding local displacement of 3.41mm. Consequently the mode of failure observed is the net tension

Figure 7. (3). Experimental test has shown initial damage in the specimen C occurred at 72% of final bearing failure. As for laminate B, the bearing response shows a small drop at the FPS point followed by a stress build-up to a SPS. But beyond the peak stress, the stress drops rapidly, faster than for laminate B. The rapid stress drop beyond the SPS, is caused by a tension failure that spreads across.

In conclusion, the diversity in laminating sequences led to equally diverse failure patterns. There are however general trends that go beyond this diversity. Perhaps the most salient general feature was that there was a first peak stress at about 4632 N, irrespective of coupon geometry and reinforcement architecture, for all the coupons that had an ultimate bearing strength greater than 4632 N. They also observed that the damage load was independent of the coupon geometry. Both bearing and shearout were observed at the damage load for the present laminates. The bearing damage caused an instant load drop and hole elongation. A steady stress build-up was therefore possible, up to the second peak load. For the standard coupon geometry, the bearing damage could only develop when enough off-axis reinforcement was present. By picking three samples geometry types, a global picture is created for the bearing behaviour of typical fiber of Carbon/epoxy laminates. The standard substrate geometry showed the most diverse failure behavior. By adding off-axis reinforcement the bearing behaviour changed from a catastrophic failure with relatively low strength to a progressive high strength failure. The development of a progressive failure was always associated with macroscopic bearing damage at the hole edge [39-40].
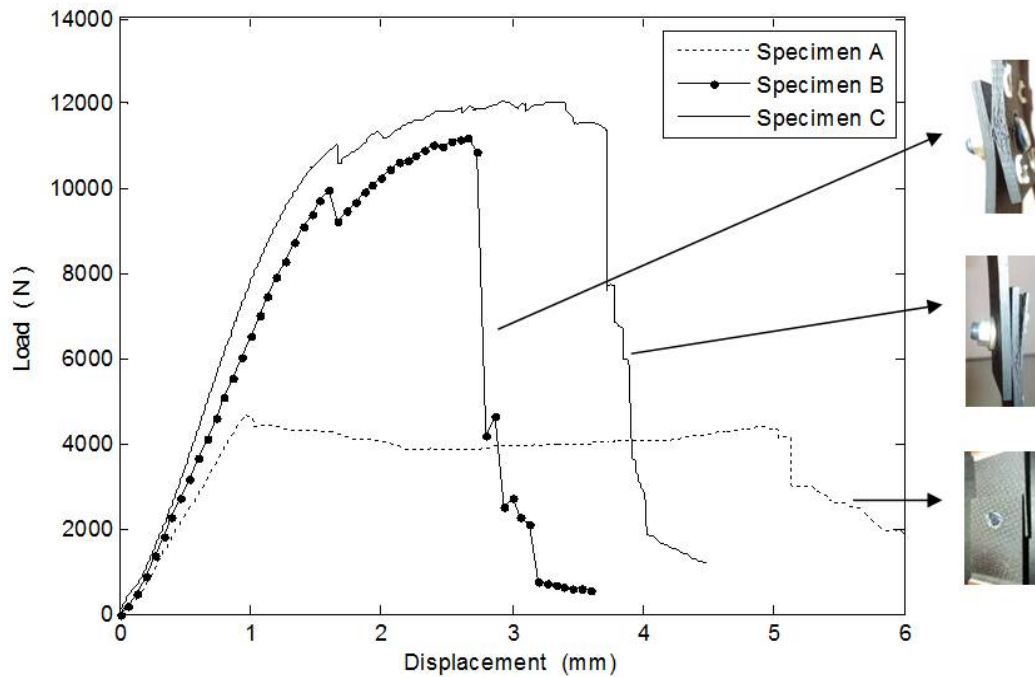
Figure.6: Loading function displacement of the three types of test specimen

The mechanical properties obtained from the tensile test are the Young's modulus E, the maximum load and the ultimate load are presented in Table 6. The Young's modulus is taken as a slope of the strain–deformation curve between 0.04% and 0.15% of strain.

The distribution of events as function of time is presented in figure 8. More important acoustic events are ranging from 40 to 65 dB, it is the matrix cracking which is characterized by short duration waveforms of long rise time and low energy [24]. The amplitude is ranging between 65 and 70 dB, less acoustic events is observed compared to the first range. From 80 dB Acoustic events become less important. It is the final rupture of fibers characterized by higher energy[26].

Table 6: Mechanical properties of the specimen C with statistical parameters.

	Young's Modulus E (MPa)	Maximum load (N)	Ultimate load (N)
Average	19520,31	12379,26	11158,94
variance	282607,89	230358,32	533757,03
Standard deviation	531,60	479,95	730,58
Absolute uncertainty	564,65	459,77	852,46
Relative uncertainty	2,89	3,71	7,63

Figure.7. Macroscopic view of post-mortem; (1) specimen A, (2) specimen B, (3) specimen C.
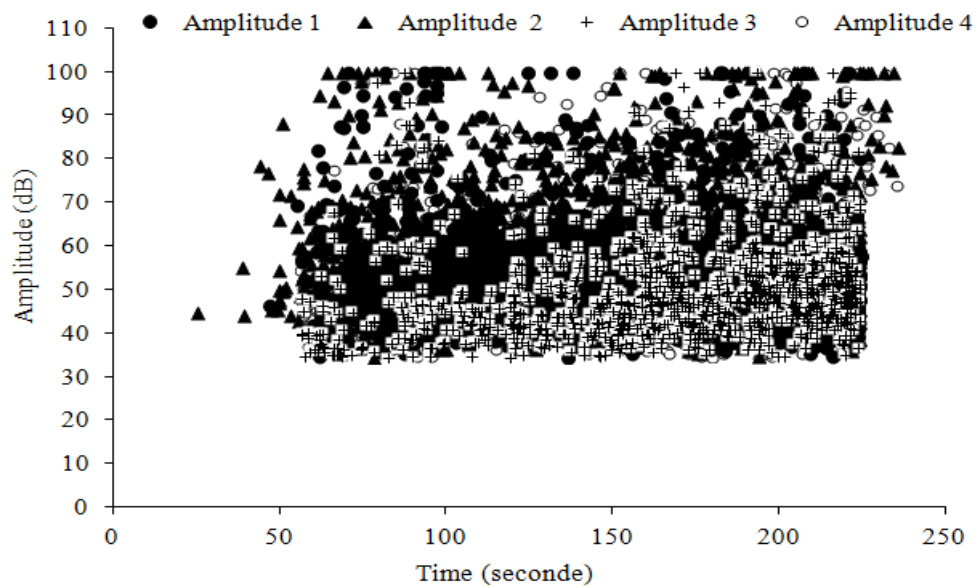

Figure.8. Distribution of events as function of time during the tensile test of the specimen C

Figure 9 illustrates the variation of the load as a function of time during a tensile test of a bolted assembly belonging to the group C, followed by the acoustic parameters as energy, cumulated count, duration and Riset. Singulars evolutions, different slopes, instantaneous deflections which occur at a point characteristic of the load/time curve are presented in figure 9 which allows the division in phases. The data files resulting from DIC allowed extracting at each load step a point of the load–displacement curve as shown in figure 10. According to the shape of the curve fig. 9 we can distinguish the following zones:

- **Zone 1** to point (a), It is followed by a transition part to the initial slope of stiffness which corresponds to the alignment of the assembly.

-**Zone 2** It is represented by the segment [a, b] and characterized by a linear elastic zone. This phase ends at the point b which corresponds to a time of 63, 28 seconds for amplitude of 44.49 dB. Quiet activity of A.E is observed in this zone.

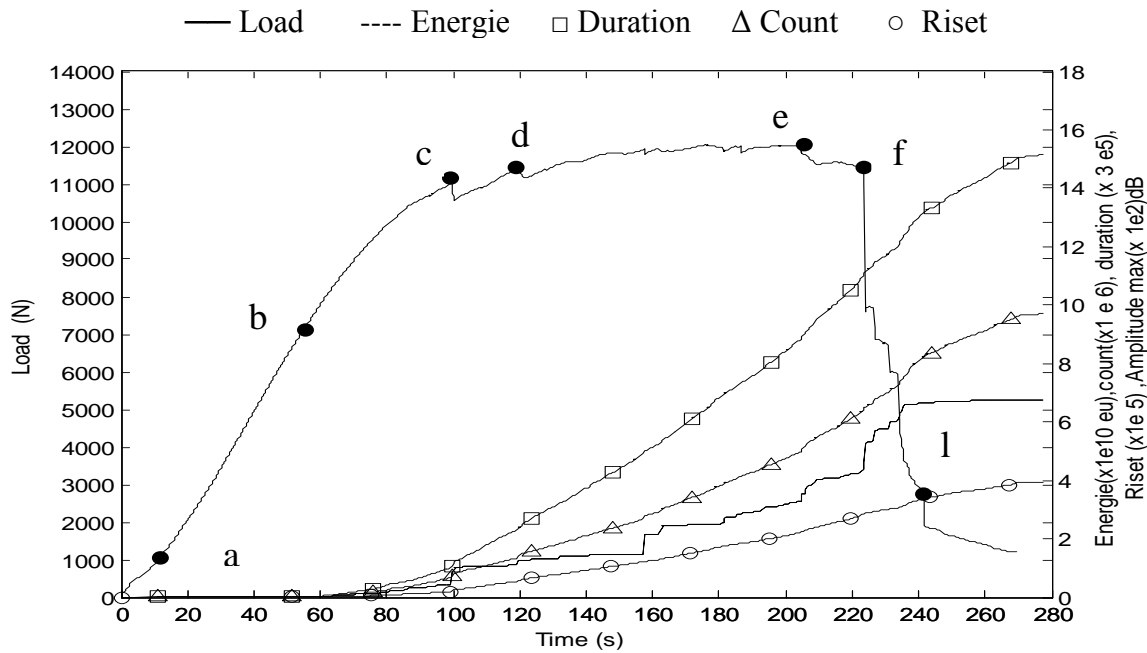— Load   ---- Energie   □ Duration   Δ Count   ○ Riset

Figure.9 Load applied against time of the specimen C followed by the acoustic parameters as energy cumulated count number the energy, duration of the signal and rise.
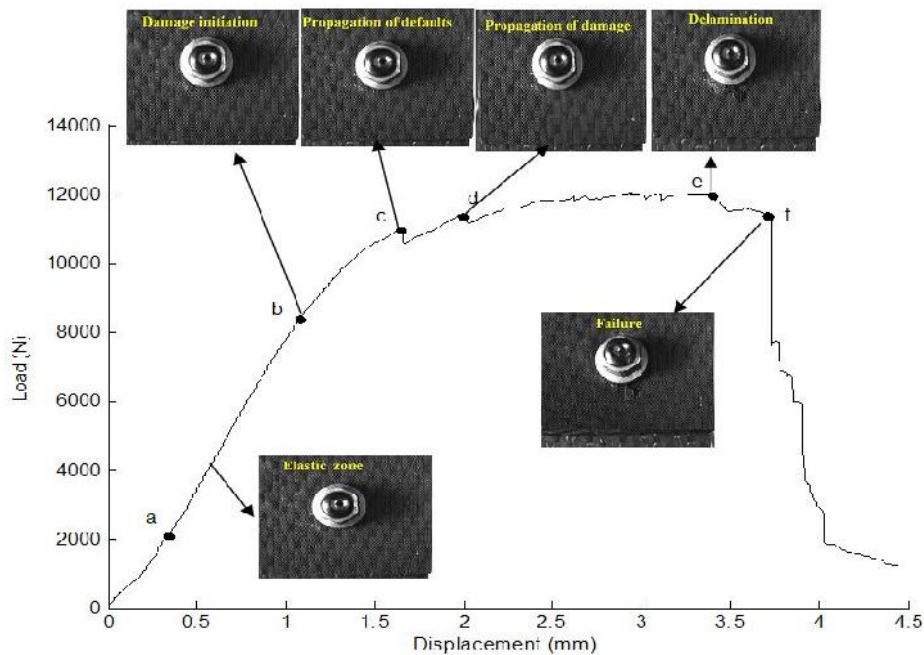

Figure.10: Images given by (D.I.C) techniques at specific point of the curve load versus time during the tensile test until failure of the specimen C

-Zone 3 is represented by the segment [b, d]. The beginning of the non-linearity of the curve at point b coincides with the occurrence of damages in the edge of the hole. It is about matrix cracking in plies 0° and micro-buckling of fibers at 45°.These defects propagate and eventually give rise to macrocracks. This phase is described by a strong acoustic emission activity marked by high values of amplitude, energy, cumulated count number, and rise time, hence more failure points and more severe damage areas were observed.

Amplitude values of b, c and d points are respectively 44, 49dB, 58, 04 dB and 67,45dB [24]. The displacement and strain field values, given by D.I.C techniques at point b, are presented in figure.11 (1) and figure 11(2). It can be seen that the strain values at point b are more important than those given for point d (Fig. 12(1) and Fig. 12(2)). In the real images given by D.I.C techniques reveals the existence of relative displacement between two substrates.

-Zone 4 is represented by the segment [d, e]. This phase corresponds to a stable distribution of the defects described by regular acoustic activities with an instantaneous leap of all acoustic parameters at point e. The plastic zone near the hole of low substrate at point (d) is highlighted by the image recorded by camera C.I.D. Significant damage was observed on the shear out plane at point (d) and delamination of plies (0° and 45°) at point d.

 -**Zone 5** is an unstable propagation zone leading to load drop and specimen failure. Acoustic activities clearly show the boundaries of the area where the maximum amplitude reaches a value of 100 dB, marking a beginning of the failure carbon fibers. This phase ends at

point (f) for the time t equal 223.28 seconds.The range values of amplitude is 80 and 100 Db , the energy, the count number, the rise time increase remarkably. The low interlaminar shear strength and transverse fibers have small effects on the longitudinal tensile proprieties, which are yet determined by longitudinal fibers. Thus, the high amplitude signals beyond 80 db representing the longitudinal fibers breakage are also mixed with middle and low-amplitude signals showing the progressive matrix cracking and interface failure. The reels images given by D.I.C techniques clearly show the delamination and fiber breakage at point (f).
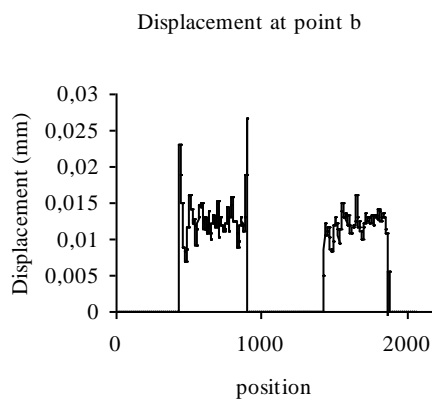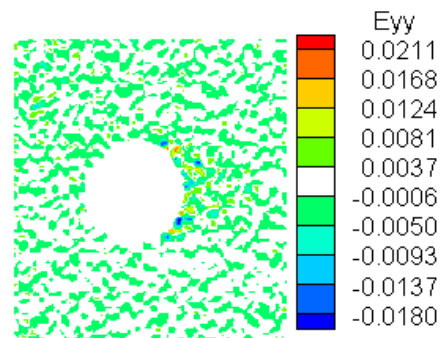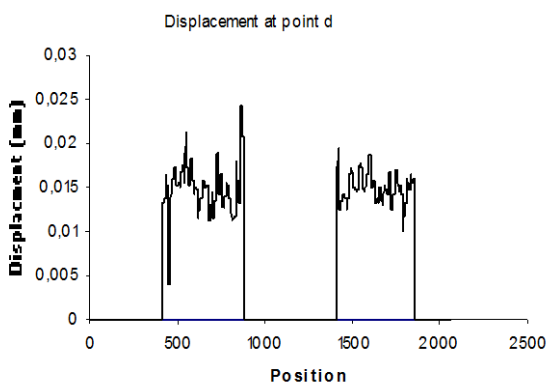
(1)   (2)
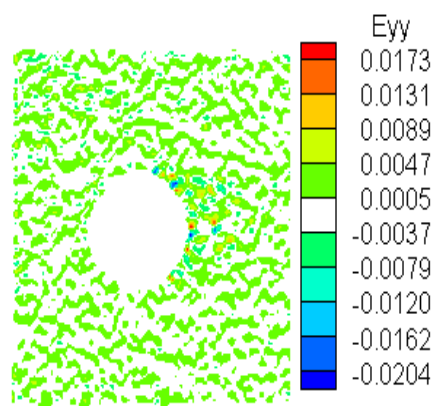
Figure. 11: (1) Field of displacements at point b, (2) the strain field at point b.along line z.

(1)   (2)

Figure.12: (1). Field of displacement at point d along line (z), (2) the strain field at point d.

.

3.1. Localization of events

To specify the positions of the localizations in the mark, we proceeded to a temporal division. Collected information is displayed for the intervals time corresponding to the acoustic activity of one or several zones. During the elastic zone, for a while t inferior to 63, 28 seconds, severs stress concentration appear around the hole location (Fig. 13. (1)). the amplitude of signals at other location is only within 40-60 dB for fibers breakage. for the time interval 206.48 < t < 223.68 corresponding to the last zone (zone 5), more locations are introduced around the hole and spread rapidly in the four area of the marker (Fig.13. (2)). These localizations confirm the presence of propagation of defaults during the tensile test until failure [22].
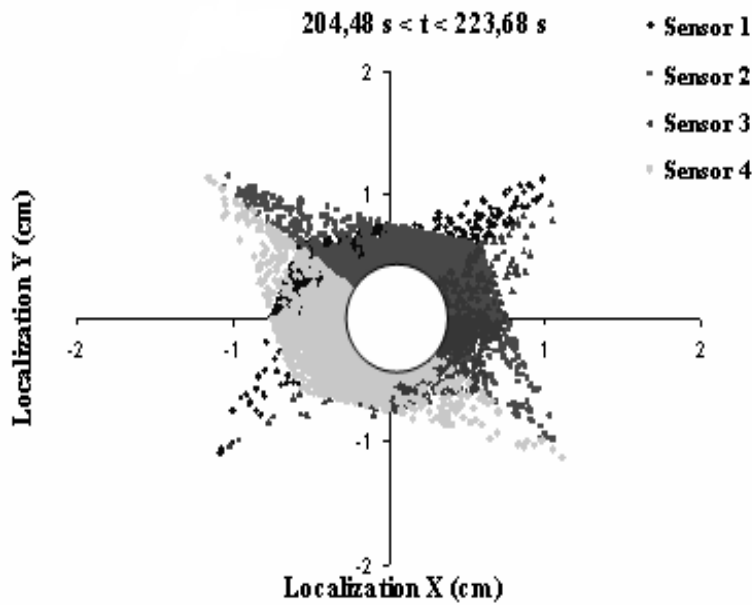
(1)
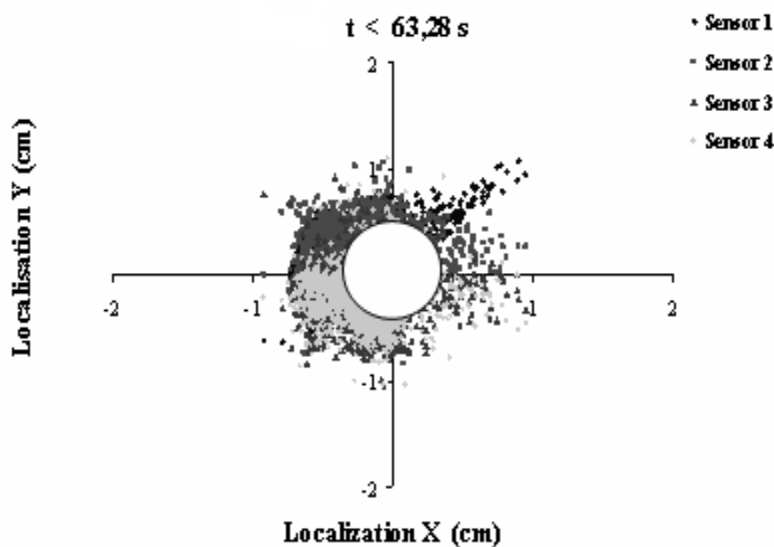
(2)

Figure.13. (1) Localizations in zone 1, (2) Localizations in zone 5.

81

3.2. Microscopic observations

In order to confirm mechanisms damage identified by acoustic emission during tensile tests, we conducted a microscopic analysis using a scanning electron microscope (SEM) on post-mortem specimens of the specimen C (Fig.14). Some specimens are additionally cut-out through their thickness. The cutting is made with a diamond disk, along the symmetry plane of the specimen.To avoid material losses and local modifications during the cutting, specimens are preliminary moulded in a coloured resin, sufficiently fluid to infiltrate inside the cracks by capillarity effect. Many mechanisms damages are observed; in the clamping area under both shoulders of the fixtures, most damages concern only the plies at 0° which are subject to plane micro-buckling.

An inter-ply delamination area can also be noticed. Outside the clamping area, plies at 0° are present out-of-plane micro-buckling. Fiber ruptures by compression can be noticed, as well as fragmentations consecutive to multiple successive micro-buckling. Due to multiple transverse cracking, an important fragmentation zone of the plies at 45° is observed. These defaults can be at the origin of inter-ply delamination once they reach the interface. Figure 15 shows enlargement of defaults as matrix cracking, delaminating and specimen C fibers breakage. In conclusion, the main rupture mechanisms giving rise to the bearing process, the load develop in front of the circular clamping area and delamination initiated by the transverse cracks in the plies at 45° can widely spread in direction of the specimen edges.
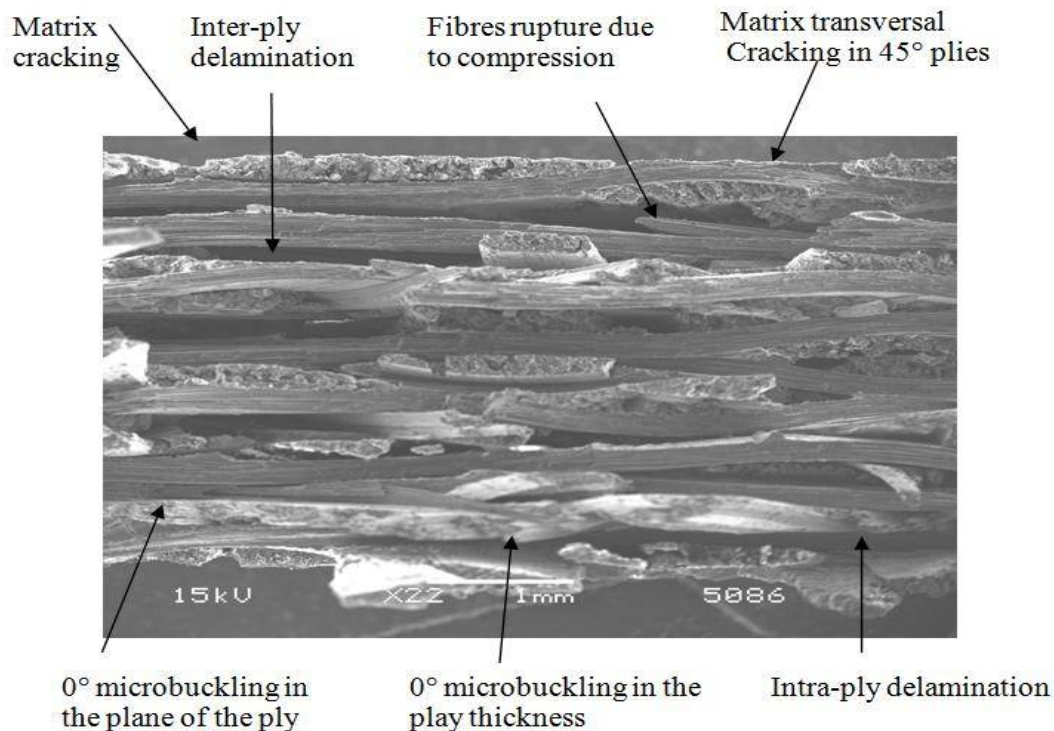

Figure 14. Microstructure of composite specimen C after fracture by scanning electron microscope.
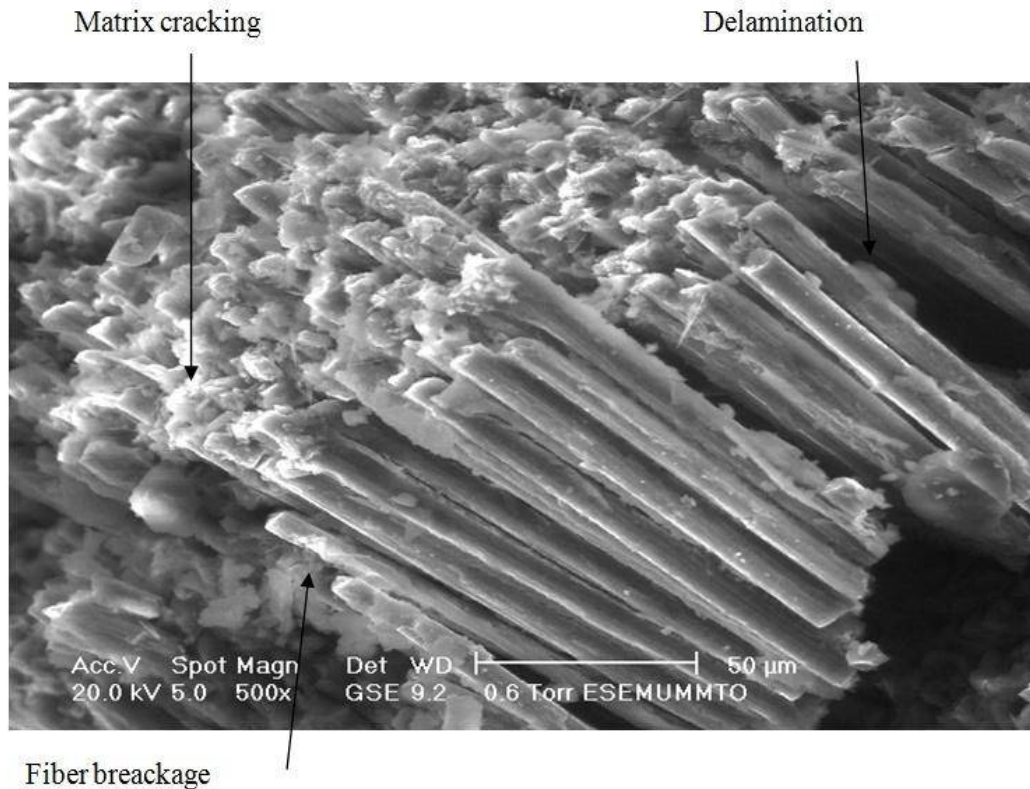
Figure.15. Magnification of microstructure of composite specimen C after fracture by scanning electron microscope.

4. CONCLUSION

The aim of this work is within the scope of the analysis by acoustic emission the mechanisms of damage and failure mode of woven composite carbon fiber/epoxy. The coupling of the acoustic emission technique (A.E) and (C.I.D) has highlighted the different phases describing the global mechanical behavior of bolted assembly.

Experimental test has shown initial damage in woven composite bolted assembly (carbon fiber /epoxy) of the specimen A, B, and C occurring respectively at 83%, 61% and 28% of final bearing failure. The damage was apparent in laminated as fiber micro buckling and through-thickness matrix cracking. The damage was concentrated on the bearing plane at the hole of edge and with increasing the load spread on the bearing side of the fastener. The fiber micro buckles were seen in the tows oriented at 0° and +45° to the applied load and the matrix cracks in the tows oriented at 45° to the applied load. Delamination appears as a direct consequence of fiber buckling and its progression generates the ruin of the laminate. Failure occurs in a hard way when stratification favors the propagation of delamination (interfaces 0°/45°). Failure modes and bearing strengths are completely influenced from stacking sequence of composite laminated plates.The analysis is supported by microscopic visualizations showing the failure mechanisms involved in the bearing process, including fragmentation, micro-buckling, delaminating and fibbers breakage.

REFERENCES

[1] Poon C. Literature review on the design of mechanically fastened composite joints, 1987. *AGARD, Conference Proceedings No. 427*, Behaviour and Analysis of Mechanically Fastened Joints in Composite Structures, Structures and Materials Panel Specialists' Meeting, Madrid, Spain, 27–29 April. p. 1.1–1.28

[2] Godwin E W, Matthews F.L, 1980. A review of the strength of joints in fiber-reinforced plastics, Part 1. Mechanically fastened joints, *Composites*, Vol.11, pp. 115-160.

[3] Camanho P P, and Matthews F.L, 1997. Stress analysis and strength prediction of mechanically fastened joints in FRP a review, *Composites Part A*, Vol.28A, pp. 29-47.

[4] Cooper C, and Turvey G.J, 1995. Effects of joint geometry and bolt torque on the structural performance of single bolt tension joints in pultruded GRP sheet materials, *Composite Structures*, Vol.32, pp. 217-226.

[5] Prabhakaran R, Razzaq Z, Devara S, 1996. Load and resistance factor design (LRFD) approach for bolted joints in pultruded composites, *Composites Part B*, Vol. 27B, pp. 351-360.

[6] Grytten F, Daiyan H, Polanco-Loria M, Dumoulin S, 2009. Use of digital image correlation to measure large-strain tensile properties of ductile thermoplastics, *Polymer Testing*, Vol.28 (28), pp. 653–660.

[7] Parsons E.M, Boyce M.C, Parks D.M, Weinberg M, 2005. Three-dimensional large-strain tensile deformation of neat and calcium carbonate-filled high-density polyethylene, *Polymer*,Vol.46 (7), pp. 2257–2265.

[8] Parsons E, Boyce M.C, Parks D.M, 2004. An experimental investigation of the large-strain tensile behavior of neat and rubber-toughened polycarbonate, *Polymer,*Vol. 45 (8), pp. 2665–2684.

[9] De Almeida O, Lagattu F, Brillaud J, 2008. Analysis by a 3D DIC technique of volumetric deformation gradients: application to polypropylene/EPR/talc composites, *Composites Part A Applied Science and Manufacturing*, Vol.39 (8), pp. 1210–1217.

[10] Eriksson I, 1990. On the bearing strength of bolted graphite/epoxy laminates, *Journal of Composite Materials*, Vol.24, pp. 1246-1269.

[11] Hollmann K, 1996. Failure analysis of bolted composite joints exhibiting in-plane failure modes, *Journal of Composites Materials*, Vol.30(3), pp. 358-383.

[12] Yan Y, Wen W D, Chang F K, and Shyprykevich P, 1999. Experimental study on clamping effects on the tensile strength of composite plates with a bolted hole. *Composites Part A,* Vol.30, pp. 1215-1229.

[13] Hart-Smith L J, 1978. Mechanically fastened joints for advanced composites, phenomenological considerations and simple analyses, Fourth Conference on Fibrous Composites in Structural Design. San Diego, California Sheraton Harbor Island Hotel, November, p. 14-7.

[14] Hart-Smith LJ, 1991. An engineer's viewpoint on design and analysis of aircraft structural joints. In International Conference on Aircraft Damage Assessment and Repair, 26-28 August, Melbourne, Australia.

[15] Ramkumar R L, Saether E S, 1985. Strength analysis of composite and metallic plates bolted together by a single fastener, Aircraft Division Report AFWAL-TR-85-3064, Northrop Corporation, Hawthorne, CA, August USA.

[16] Tang X, Whitcomb JD, 2003. Progressive failure behavior of 2D woven composites, *Journal of Composite Materials*, Vol.37 (14), pp. 1239–1259.

[16] Tang X, Whitcomb JD, 2003. Progressive failure behavior of 2D woven composites, *Journal Composite Materials*, Vol.37(14), pp. 1239–59.

[17] John S, Herszberg I, Coman F, 2001. Longitudinal and transverse damage taxonomy in woven composite components, *Composites Part B*, Vol.32, 659–668.

[18] El Hage C, 2006. Modélisation du comportement élastique endommageable des matériaux composites a renfort tridimensionnel, Thèse de doctorat, Laboratoire Roberval. Compiègne, Université de Technologie de Compiègne, France 333p

[19] Kurashiki T, Zako M, and Verpoest I, 2002. Damage development of woven fabric composites considering an

effect of mismatch of lay-up, Proceedings of the 10th European conference on composite materials (ECCM-10).

[20] Uetsuji Y, Zako M, Nishiyabu K, 2002. Numerical analysis and in-situ SEM observation of damage development for woven fabric composite materials, *Journal of the Society of Materials Science*, Vol.51(10), pp. 1147–53.

[21] Sugimoto K, Nakai A, and Hamada H, 2004. Effect of lamination sequence on mechanical behaviour of woven composites, Proceedings of the 7th international conference on textile composites (TexComp-7), p. 1–4

[22] T. Dang Hoang, C. Herbolot, A. Imad, 2010. Rupture and damage mechanism analysis of a bolted assembly using coupling techniques between A.E. and D.I.C, *Engineering Structures,* Vol.32, pp. 2793-2803

[23] Chen O, Karandika P, and Takeda N. 1992. Acoustic emission characterization glass-matrix composite, *Non destructive Testing and Evaluation*, Vol. 8-9, pp. 869-878.

[24] Kim, S.T, Lee and Y.T, 1997. Characteristics of damage and fracture process of carbon fiber reinforced plastic under loading-unloading test by using AE method, *Materials Science and Engineering*, Vol.A, pp. 234-236.

[25] Karger Kocsis, J., Harmia T, and Czigany T, 1995. Comparison of the fracture glass mats, *Composites science and Technology*, Vol.54, pp. 287-298.

[26] Kotsiko G, Evans J. T, and Gibson A. G, 2000. Environmentally enhanced fatigue damage in glass fiber reinforced composites characterized by acoustic emission, *Composites Part A*, Vol.5(31), pp. 969-977.

[27] Ceysson O, Salvia M, and Vincent L, 1996 damage Mechanisms characterization and acoustic emission analysis, *Scripta Materialia*, Vol.34(8), pp. 1273-1280.

[28] Benzeggagh M.L, Barre S, and Echalier B, 1992. Etude de l'endommagement de matériaux composites à fibres courtes et à matrice thermoplastique, journées Nationales des composites, on AMAC, pp. 703-714. Paris.

[29] Mouhmid B, Imad A, Benseddiq N, and Le Compte D, 2009. In experimental analysis of fracture mechanism of short glass reinforced polyamide 6,6 (SGFR-PA), *Composites Science and Technology*, Vol.69, pp. 2521-2526.

[30] Uenoya T, 1995. Acoustic emission analysis on interfacial fracture of laminated fabric polymer composites, *Journal of Acoustic Emission*, Vol.13, S95-S102.

[31] Hill, V K, Walker II, J. L. and Rowell, G. H, 1996. Burst pressure prediction in graphite/epoxy pressure vessels using neural networks and acoustic emission amplitude data, *Materials Evaluation*, Vol.54(6), pp.744-748

[32] Huguet S, Godin N, and Gaertener R, 2002. Use acoustic emission to identify damage modes in glass fiber reinforced polyester , *Composites Science and Technology*, Vol.62, pp. pp. 1433-1444.

[33] Godin N, Huguet S, and Gaertner R, 2003. Clustering of emission acoustic signals collected during tensile tests on unidirectional glass/polyester composite using supervised and unsupervised classifiers, *NDT & E international independent non destructive testing and evaluation*, Vol.37, pp. 253-265

[34] Mai YW, Cotterell B, Horlyck R, Vigna G, 1987. The essential work of plane stress ductile fracture of linear polyethylenes. Polym Eng Sci;27 (11), pp. 804–9.

[35] Peters WH, Ranson WF, Sutton MA, 1983. Application of digital correlation methods to rigid body mechanics, *Opt Eng;*22 (26), pp. 427–31.

[36] Sutton MA, Wolters WJ, Peters WH, Rawson WF, McNeil SR, 1983. Determination of displacement using an improved digital image correlation method. *Image Vision Comput*;1(3), pp. 133– 139.

[37] Jean N P, Hugo L, Stéphane R, François H, 2009. Digital image correlation and biaxial test on composite material for anisotropic damage law identification, *International Journal of Solids and Structures,* 46, pp. 2388–2396.

[38] Mostafapour A, Davoodi S, Ghareaghaji M, 2014. Acoustic emission source location in plates using wavelet analysis and cross time frequency spectrum, *Ultrasonics* 54, pp. 2055–2062.

[39] Manuel P , Eric D, David D , Daniel C, 2008. Experimental failure analysis of mechanically fastened joints with clearance in composite laminates under preload. *Composite Structures* 84, pp. 99–113.

[40] Vangrimde B, Boukhili R, 2003. Descriptive relationships between bearing response and macroscopic damage in GRP bolted joints, *Composites*, Part B 34, pp. 593–605.

Nomenclature

F   Load [Newton];
A Amplitude [decibel] ;
t   time [second] ;
E Energy [eu] ;
D   Hole diameter [mm] ;
W Wide of substrate [mm];
L   Length [mm];
q Thickness of substrate [mm];
e   Edge distance [mm];
d   Displacement[mm];
σ Strength [MPa];
ε Elongation [%];
E   Young's modulus [GPa];
ν Poisson coefficient
G   Shear modulus [GPa];
G_{Ic} Toughness [J/m^3];
ρ Density [Kg/m^3];
V   Wave Velocity